

Alma Mater Studiorum Università di Bologna  
Archivio istituzionale della ricerca

Electronic Transport in the Biopigment Sepia Melanin

This is the final peer-reviewed author's accepted manuscript (postprint) of the following publication:

*Published Version:*

Reali M., Gouda A., Bellemare J., Menard D., Nunzi J.-M., Soavi F., et al. (2020). Electronic Transport in the Biopigment Sepia Melanin. ACS APPLIED BIO MATERIALS, 3(8), 5244-5252 [10.1021/acsabm.0c00373].

*Availability:*

This version is available at: <https://hdl.handle.net/11585/782499> since: 2023-06-20

*Published:*

DOI: <http://doi.org/10.1021/acsabm.0c00373>

*Terms of use:*

Some rights reserved. The terms and conditions for the reuse of this version of the manuscript are specified in the publishing policy. For all terms of use and more information see the publisher's website.

This item was downloaded from IRIS Università di Bologna (<https://cris.unibo.it/>).  
When citing, please refer to the published version.

(Article begins on next page)

This is the final peer-reviewed accepted manuscript of:

**Realì, M., Gouda, A., Bellemare, J., Ménard, D., Nunzi, J.M., Soavi, F., Santato, C.,  
Electronic Transport in the Biopigment Sepia Melanin. 2020, ACS Appl. Bio Mater.  
3, 5244–5252**

The final published version is available online at:

<https://doi.org/10.1021/acsabm.0c00373>

Terms of use:

Some rights reserved. The terms and conditions for the reuse of this version of the manuscript are specified in the publishing policy. For all terms of use and more information see the publisher's website.

*This item was downloaded from IRIS Università di Bologna (<https://cris.unibo.it/>)*

***When citing, please refer to the published version.***

# Electronic Transport in the Biopigment Sepia Melanin

*M. Reali<sup>1</sup>, A. Gouda<sup>1</sup>, J. Bellemare<sup>1</sup>, D. Ménard<sup>1</sup>, J. M. Nunzi<sup>2,3</sup>, F. Soavi<sup>4</sup>, C. Santato<sup>1\*</sup>*

<sup>1</sup>Department of Engineering Physics, Polytechnique Montreal, Montreal, H3C 3A7, Canada

<sup>2</sup>Department of Physics, Engineering Physics & Astronomy, Queen's University, Kingston, K7L 3N6, Canada

<sup>3</sup>Department of Chemistry, Queen's University, Kingston, K7L 3N6, Canada

<sup>4</sup>Department of Chemistry “Giacomo Ciamician”, Alma Mater Studiorum Università di Bologna, Bologna, 40126, Italy

**KEYWORDS.** Sepia melanin, electronic transport, reversible resistive switching, bio-sourced materials, sustainable (green) organic electronics

## **Abstract**

Eumelanin is the most common form of the pigment melanin in the human body, with diverse functions including photoprotection, antioxidant behavior, metal chelation, and free radical scavenging. Melanin also plays a role in melanoma skin cancer and Parkinson’s disease. *Sepia Melanin* is a natural eumelanin extracted from the ink sac of cuttlefish.

Eumelanin is an ideal candidate to eco-design technologies based on abundant, biosourced and biodegradable organic electronic materials, to alleviate the environmental footprint of the electronics sector.

Herein, the focus is on the reversible electrical resistive switching in dry *Sepia* eumelanin pellets, pointing to the possibility of predominant electronic transport a *conditio sine qua non* to develop melanin- based electronic devices. These findings shed new light on the possibility to describe the transport physics of dry eumelanin by the amorphous semiconductor model. Results are of tremendous importance for the development of sustainable organic electronics.

## **Introduction**

The rapidly growing demand for consumer electronics, one of the most ubiquitous technologies, has led to unsustainable amounts of waste of electrical & electronic equipment (WEEE). On a global scale, WEEE amounts approximately to 45 megatons per year.<sup>1</sup> WEEE contains hazardous substances that pose health and environmental concerns.<sup>1</sup> Refurbishment, recycling and recovery in conventional (inorganic) electronics are viable routes to limit the environmental footprint of consumer electronics.<sup>2</sup> In parallel, the eco-design of electronic devices based on the use of abundant organic bio-sourced materials that are potentially biodegradable, a field that we call organic green (sustainable) electronics, is of the utmost importance, e.g. for the development of low human- and eco-toxicity technologies for the Internet of Things.

In the melanin biopigment family, eumelanin is a brown-black subgroup found in the human body, other mammals, birds, reptiles, amphibians and fishes as well as in lower invertebrates, such as cuttlefish and insects.<sup>3</sup> In humans, aside from photo-protection, eumelanin is involved in

a variety of processes, e.g. the accumulation and release of metal cations in the body.<sup>4,5</sup> It is noteworthy that the interactions between iron and neuromelanin, a pigment made of eumelanin and red-yellow pheomelanin, present in the brain of humans and primates, have been related to Parkinson's disease.<sup>6</sup> The remarkable adhesion of melanin-like materials on surfaces is the underpinning for emerging applications in the biomedical and water treatment fields.<sup>7-9</sup> Sepia melanin is a natural eumelanin extracted from the ink sac of cuttlefish (*Sepia officinalis*).<sup>10</sup>

Eumelanin is an ideal bio-sourced candidate for the exploration of the potential of sustainable organic electronics. Indeed, its molecular structure features electronic conjugation (alternance of single and double bonds), which is a peculiar structural feature of organic semiconductors.<sup>11</sup> At the same time, beyond its ubiquity among flora and fauna, eumelanin is biocompatible, edible and potentially biodegradable.<sup>7,12</sup> Considering the presence of redox active quinone groups in the molecular structure,<sup>7</sup> electronics powered by eumelanin-based electrochemical energy storage devices can also be conceived. Indeed, the redox activity of eumelanin has recently enabled a number of technologies, such as melanin-based biological electrodes as well as flexible and light-assisted (micro)supercapacitors.<sup>13,14</sup>

Eumelanin is made up of two building blocks, 5,6-dihydroxyindole (DHI) and 5,6-dihydroxyindole-2-carboxylic acid (DHICA), coexisting in different redox states. Hydroquinone (H2Q) is the reduced state, semiquinone (SQ) the intermediate redox state and quinone (Q) the oxidized state (**Scheme 1**). The presence of water shifts towards the right the comproportionation equilibrium where H2Q and Q react to give SQ extrinsic radicals and protons. The latter are the mobile electronic charge carriers in eumelanin <sup>15</sup> (**Scheme 2**).

DHI and DHICA have several polymerization sites making eumelanin a chemically heterogeneous macromolecule.<sup>16,17</sup> This heterogeneity explains the short-range order in the

material that can therefore be defined, to a certain extent, as amorphous. Nevertheless, self-assembled  $\pi$ - $\pi$  stacked supramolecular structures with a characteristic inter-plane spacing of  $\sim 3.7$  Å have been observed both with natural and synthetic eumelanin.<sup>18</sup>

In the 1970s, McGinness et al. reported on the reversible electrical resistive switching from a high (OFF) to a low (ON) resistive state observable beyond a threshold voltage ( $V_T$ ) for hydrated eumelanin pressed pellets.<sup>19</sup> At that time, resistive switching had been experimentally observed in amorphous Si, amorphous Ge and chalcogenide glasses (e.g. amorphous Te and amorphous Se).<sup>20</sup> As a result, the resistive switching behavior shown by eumelanin pellets was interpreted within the Mott-Davis amorphous semiconductor model (ASM).<sup>19,21</sup> This model also provided an explanation for the broadband UV-Vis absorption of the biopigment.<sup>22</sup> A crucial element in the work of McGinness et al. was the observation that only hydrated eumelanin pellets exhibited electrical resistive switching, i.e. dry pellets did not. The lack of switching of dry pellets was explained by the modified dielectric constant theory, which posits that the adsorbed water increases the dielectric constant of the material, lowering the activation energy for charge transfer processes.<sup>23</sup> Recent publications on the electrical response of hydrated eumelanin<sup>24–26</sup> questioned the ASM and proposed the mixed ionic-electronic conductor model (**Scheme 2 and Table 1**).<sup>27–29</sup>

Here, we report on the observation of predominant electronic transport in dry pellets of natural Sepia melanin, processed at room temperature. Pellets exhibit room temperature conductivity of about  $10^{-3}$  S·cm<sup>-1</sup>, after switching. Our observation has profound implications for the development of the field of sustainable organic electronics. Indeed, the observation of pure electronic transport paves the way towards the development of Sepia melanin-based transistors

and memory devices. Further, long-term implications are also foreseen in the medical and biomedical fields.

## Experimental Section

### *Sepia melanin extraction*

Sepia melanin was extracted from the ink sac of the cuttlefish *Sepia officinalis*. First 100 g of ink were suspended in 200 mL of HCl 2M and stirred for 24 hr at 10 °C. The suspension was centrifuged in a planetary mixer (THINKY ARM-310) and washed several times with 0.5M HCl, ethanol, DI water, ethyl acetate and a buffer solution (0.95 v/v of monobasic sodium phosphate 200 mM, 40.5 v/v of dibasic sodium phosphate 200 mM, 50 v/v of DI water). For each step, the suspension was weighed, and the pH measured. Centrifugation was performed at 10000 rpm at 5 °C (25 min for DI water and buffer solution, 15 min for HCl 0.5M, ethanol and ethyl acetate). After stirring, the centrifugate was sequentially washed with HCl 0.5M, DI water, the buffer, and ethanol, and centrifuged at each washing step. Subsequently, the suspension was washed again with DI water and centrifuged three times. The final product was lyophilized for 24 hr to remove solvents. A fine black powder was finally obtained.

### *Fabrication of Wet Pellets*

The *Sepia* melanin powder was ground to remove large agglomerates and subsequently weighed (analytical balance, accuracy  $10^{-5}$  g). For the hydrated pellets, we measured the weight percent gained by the pellets after 24 hr hydration (% wt), at different percentages of relative humidity in the atmosphere (**Table S1**). The percentage of weight gained after hydration was calculated using the following relation:  $\%wt = \frac{W_2 - W_1}{W_1} \times 100$ , where  $W_2$  and  $W_1$  are the weight after and before hydration respectively. The hydration was performed in a Cole-Parmer Mini

Humidity Chamber (03323-14) equipped with an automatic humidity controller and an ultrasonic humidification system (control humidity levels from 20% to 90% with programmable set points).

A cylindrical stainless-steel coin cell (inner diameter 15.5 mm, outer diameter 19.5 mm, thickness prior pressing 2.6 mm) was used as protective gasket to assemble and seal the pellet. The coin cell was assembled as follows. A pre-cleaned 99% purity Cu foil (dimensions of the inner diameter of the coin cell, 0.1 mm thickness), from Goodfellow Cambridge Limited, was placed inside the coin cell and the hydrated powder gently transferred on the Cu surface. The top contact was then made by placing the top stainless-steel disk (0.1 mm thickness, SUS316L from SteelJIS) on the powder and the sandwich structure sealed with the upper cap (**Scheme 3B**). The coin cell was then manually pressed into 2 mm thick pellets by applying a pressure of 3 tons for 60 s by means of a manual hydraulic press machine (Specac's Atlas Series).

#### *Fabrication of Dry Pellets*

Sepia melanin powder was ground to remove large agglomerates and transferred with the coin cell and the pre-cleaned contacts to an argon glovebox ( $\text{H}_2\text{O} < 0.1$  ppm, equipped with a manual hydraulic press machine where it was kept for 24 hr prior to pressing it into pellets. The powder was weighed (analytical balance, accuracy  $10^{-5}$  g) and the coin cell assembled following the same fabrication procedure as the hydrated samples. The structure was then pressed into 2 mm thick pellets (3 tons for 60 s).

#### *Electrical*

The pellets were clamped to ensure the stability of the contacts during the electrical measurements. Then, they were connected to an amperometer at the terminals of which the current was recorded. The pellets were modeled with an electrical resistance ( $R_p$ , including the



contact resistance) in series with the internal resistance of the voltage source  $R_S$ . At the threshold voltage ( $V_T$ ),  $R_P$  can be calculated as  $R_P = \frac{V}{I} - R_S$ , where  $V$  is the applied voltage,  $I$  the measured current and  $R_S$  the internal resistance of the voltage source (**Scheme 3A**). The electrical response of the pellets was acquired using a Genesys™ Lambda-TDK 600-2.6 DC power supply (output voltage 600 V, maximum output current 2.6 A). *LabView I-V Software* was used for data recording and programmed to limit the current of the power supply (output current) to the maximum value supported by the resistor (about 150 mA, **Scheme 3A**). The room temperature electrical conductivity of the pellets can be calculated using the following equation:

$$\sigma(295K) = \frac{t}{A \times R_p} \quad (1)$$

where  $t$  is the thickness,  $A$  is the inner surface area and  $R_p$  is the resistance of the pellets.

### *Chemical*

Before and after the electrical tests, the chemical properties of the hydrated and dry pellets were characterized via Raman Spectroscopy and X-ray Photoelectron Spectroscopy (XPS). For the former, we used a Renishaw InVia Raman spectrometer ( $\lambda=514$  nm, 100 nm s<sup>-1</sup> scanning rate, 5% of the total power to prevent overheating effects). XPS was performed with a VG ESCALAB 3 MKII apparatus (source Mg K $\alpha$ , power 300 W [15 kV, 20 mA], pressure in analysis chamber ca. 10<sup>-9</sup> Torr, electron take off angle 0 deg, analyzed depth less than 10 nm, detection limit 0.1% at). Survey scans and high-resolution scans were carried out with 1 eV and 0.05 eV energy steps. Background subtraction was performed via the *Shirley method* and charge correction with respect to C<sub>1s</sub> set at 284.7 eV.

### *Electrochemical Impedance Spectroscopy*

EIS measurements were performed at ambient conditions with a BioLogic bipotentiostat (SP-300). Data were acquired at open circuit potentials (OCP), within the frequency range 3 MHz - 0.1 Hz, 20 points per decade, 10 mV oscillation amplitude.

### *Scanning Electron Microscopy (SEM) and Energy-Dispersive X-ray (EDX)*

A JEOL JSM7600F microscope was used. EDX was carried out using the same microscope with Aztec (Oxford) software, detector x-Max (80 mm<sup>2</sup>, Oxford), at 5 kV.

## **Results**

### *Electrical response of Sepia melanin pellets*

The current-voltage characteristics of dry and wet Sepia melanin pellets, placed between Cu and stainless-steel electrodes, show that for dry pellets, during the first current-voltage scan, the current monotonically increases with the increase of the voltage up to the threshold voltage  $V_T$ , where the electrical resistive switching takes place (**Figure 1A**). The resistance across the pellets in the ON and OFF states is about 100  $\Omega$  and 550  $\Omega$  (the ON resistance,  $R_{ON}$ , is calculated at the maximum value of the current after switching, whereas the OFF resistance,  $R_{OFF}$ , is calculated at  $V_T$  right before switching (see experimental section and **Table S2**). For an ON resistance of 100  $\Omega$ , dry pellets feature a room temperature electrical conductivity of about  $1 \times 10^{-3} \text{ S}\cdot\text{cm}^{-1}$ , a value falling within the range of electrical conductivity of semiconductors.

From the second current-voltage cycle, the electrical response is significantly different from that of the first. Indeed, the response fits a current-voltage power law of the form  $I \propto V^a$ , with values of  $a$  being close to or higher than unity (**Figures S1 A and C and Table S3**). The

electrical response of dry pellets features the same current-voltage power law at different voltage scan rates, after the first scan (**Figure 1C**). The independence of the electrical response on the voltage scan rate suggests predominant electronic conduction in the dry pellets. Values of  $a \geq 1$  in the power law indicate that, under the effect of an electric field, electronic space charge layers, broadly defined as an excess of electrons or holes over a region of space, form at the Sepia melanin/metal interface. Amorphous materials, such as eumelanin, are prone to host space charge layers due to the presence of structural defects acting as charge carrier traps.<sup>30,31</sup>

Wet Sepia melanin pellets also feature electrical resistive switching (**Figures 1B, S1 B and D**). No considerable difference is observable between the first and the following scans apart from  $V_T$  (**Figure S1 D**). The scan rate has a dramatic effect on the current-voltage characteristics of wet pellets. The electrical response shows that, beyond  $2000 \text{ mVs}^{-1}$ , the resistive switching is not observable, and the electrical response fits a power law (**Figures 1D, S2 and Table S3**). From these results, we infer that conduction in wet pellets is predominantly electronic at high voltage scan rates.

After the resistive switching, we followed the evolution of the resistance with time, for dry and wet pellets (**Figure S3**). Dry and wet pellets have an initial resistance of  $130 \text{ } \Omega$  and  $225 \text{ } \Omega$ . The resistance of dry and wet pellets increases up to about  $1200 \text{ } \Omega$  in 10 hr (in the first 5 hr the resistance of the dry pellets increases by ca.  $27 \text{ } \Omega \text{ hr}^{-1}$  while the resistance of the wet counterparts by ca.  $155 \text{ } \Omega \text{ hr}^{-1}$ ). Such an increase of resistance with time points to volatile memory behavior of both dry and wet Sepia melanin pellets, analogous to organic polymer-based memory devices.<sup>32</sup> To gain insights into the relaxation processes taking place after resistive switching, we measured the current-time characteristics at constant electrical bias. Dry pellets show a plateau-like behavior after an initial increase of the current, most likely attributable to an electric field-

induced supramolecular arrangement favorable to electronic transport (**Figure 2**).<sup>33</sup> On the other hand, the transient current characteristics of wet pellets show an exponential decay likely due to the formation of ionic double layers, followed by a plateau-like behavior attributable to electronic transport (**Figure 2 and Table S4**).

### *Electrochemical Impedance Spectroscopy*

To shed light on ionic and electronic processes featuring different relaxation times, as well as possible interfacial processes at Sepia melanin/metal interfaces, we performed an Electrochemical Impedance Spectroscopy (EIS) study with frequency ranging from 3 MHz down to 0.1 Hz. Nyquist plots (imaginary vs real components of the complex impedance) obtained from dry pellets before resistive switching feature one semicircle and a low-frequency diffusion tail (**Figure 3A**). We associate the high-frequency semicircle with the electronic impedance of the dry pellet and the Sepia melanin/metal electrode interfacial impedance. The low-frequency tail describes electronic diffusion processes in dry Sepia melanin (suggesting the hypothesis that ionic contribution can be excluded). Assuming a simple resistor-capacitor behavior (RC) with a semicircle, a relaxation time of 17.4 ms is obtained (this is the  $1/f_{\text{max}}$  value where  $f_{\text{max}}$  is the frequency of the top of the semicircle, about 57.5 Hz). On the other hand, Nyquist plots of the wet pellets before resistive switching exhibit three semicircles with relaxation times of 1.33  $\mu\text{s}$ , 0.31 ms, 6.14 ms (**Figure 3C**). We propose that the two high-frequency semicircles are attributable to the ionic and electronic impedance in the bulk whereas the low-frequency one is attributable to the charge transfer impedance at the Sepia melanin/metal interfaces. The presence of three semicircles suggests electronic conduction in parallel with ionic conduction.<sup>34,35</sup> The overall impedance should include the capacitance developing at the interface. Nyquist plots of

wet and dry pellets do not show any low-frequency capacitive line. Considering the thickness of the pellets (ca. 2 mm, see experimental section), the capacitance is expected to be insignificant. Before the electrical resistive switching, wet pellets show lower impedance than their dry counterparts. This observation can be rationalized in terms of the comproportionation equilibrium, which induces a high density of SQ extrinsic radicals and protons in wet pellets with respect to dry ones, and leads to the decrease of ionic and electronic impedance.<sup>27</sup>

After the electrical resistive switching, we observe that dry and wet pellets exhibit only one semicircle in the EIS spectra (**Figures 3B and D**). The buildup of an electrical double layer under the action of the electric field, expected to be electronic for dry pellets and predominantly ionic for their wet counterparts, likely facilitates charge carrier injection in the two types of pellets, thus leading to similar EIS responses. We also observe that the real part of the total impedance of wet pellets, after the electrical resistive switching, is higher than that of dry pellets. This observation could be attributed to possible side reactions at the wet Sepia melanin/metal interface that passivate the metal contacts.

### *Scanning Electron Microscopy*

To evaluate the possibility of explaining the resistive switching by the formation of metallic conductive filaments bridging the interelectrode distance by electrode dissolution,<sup>20,24</sup> we investigated the surface of the electrodes after switching by Scanning Electron Microscopy (SEM). SEM images and Energy Dispersive X-ray spectra (EDX) do not show any trace of metallic filaments (**Figures S4 and S5**). Therefore, we tentatively exclude the formation of metallic filaments as the cause of the resistive switching.

### *Raman Spectroscopy*

We evaluated the possibility of attributing the resistive switching to a phase transition from amorphous to graphitic carbon by Joule heating.<sup>20</sup> To this end, we performed Raman spectroscopy surveys of dry and wet Sepia melanin powder samples obtained from pellets before and after resistive switching. Raman spectra of dry and wet Sepia melanin do not show any change before and after switching. We did not observe any peak or shoulder attributable to ordered sp<sup>2</sup> carbon (**Figures S6 A, B, C and Table S5**).<sup>36</sup>

### *X-ray Photoemission Spectroscopy and X-ray Diffraction*

In agreement with the results of Raman spectroscopy, the high-resolution C1s X-ray photoemission (XPS) spectra of dry Sepia melanin powders, acquired before and after the current-voltage measurements, do not show evidence of graphitic carbon (**Figures S6 D and E, Tables S6 and S7**).

X-ray Diffraction (XRD) patterns of dry Sepia melanin powders before and after the electrical resistive switching do not show any signature of graphitic planes (**Figure S7**).<sup>37</sup>

## **Discussion**

We propose a tentative model to explain our results, based on the hypothesis that in dry pellets charge carrier injection takes place at sufficiently high applied voltages causing the formation of space charge layers namely *electronic* double layers at the Sepia melanin/metal interface (**Scheme 4**). A further increase of the voltage leads to traps filling<sup>30,31</sup> and to the effective overlap of the tails of the functions describing the density of energy states of the valence and conduction bands, eventually leading to the resistive switching.<sup>20</sup> In our model, the tails stem

from the amorphous nature of the Sepia melanin material. From the second current-voltage scan, dry pellets are in a trap-free regime and the current-voltage characteristics can be described by a power law.<sup>20</sup> For the wet pellets, space charge layers with ionic nature at the Sepia melanin/metal interfaces would lead to the electrical resistive switching (**Scheme 4**). The mixed protonic-electronic conductor model for the wet pellets is supported by the linearization of the current-voltage characteristics at voltage scan rates higher than 2000 mVs<sup>-1</sup>. Work is in progress to locate the Highest Occupied Molecular Orbital (HOMO) and Lowest Unoccupied Molecular Orbital (LUMO) energy levels of Sepia melanin, by Ultraviolet Photoelectron Spectroscopy (UPS) and Inverse Photoemission Spectroscopy (IPES), with the aim to optimize the charge carrier injection process.

## Conclusion

In conclusion, dry and wet Sepia melanin pellets included between metal electrodes feature reversible electrical resistive switching. Our dry and wet pellets feature a conductivity of about 10<sup>-3</sup> S·cm<sup>-1</sup> after switching. This value refers to natural eumelanin pellets processed at room temperature. We propose that in *dry* Sepia melanin pellets, under bias, the effective overlap of the density of energy states of valence and conduction band leads to the electrical resistive switching. Electrical double layers (expected to be electronic in dry pellets and ionic in wet ones) enable charge carrier injection at the Sepia melanin/metal interface. This behavior points to the validity of the amorphous semiconductor model to describe the transport physics of dry Sepia melanin. The linearization of the current-voltage characteristics after switching and at different voltage scan rates is a strong indication of predominantly electronic conduction. However, the buildup of ionic double layers at voltage scan rates below 2000 mVs<sup>-1</sup> and the linearization of the current-voltage characteristics at higher voltage scan rates support the mixed protonic-electronic

conduction model to describe the transport physics of *wet* Sepia melanin pellets, in agreement with the literature.

The observation of predominant electronic transport in Sepia melanin satisfies the *conditio sine qua non* to start designing and developing Sepia melanin-based devices. Our results are of the highest importance for the development of the field of sustainable organic electronics that aims at alleviating the environmental footprint of the electronics sector using abundant, solution processable, possibly biodegradable electronic materials, including biomolecules extracted from agri-waste and biomass feedstock.

### **Supporting Information**

Sequential current-voltage scans and cycles of Sepia melanin pellets (**Figures S1 and S2**), mapping of resistance as a function of time in unbiased condition for Sepia melanin pellets (**Figure S3**), SEM and EDX analysis of copper and stainless-steel electrodes (**Figures S4 and S5**), Raman spectroscopy and XPS survey of Sepia melanin pellets (**Figure S7**), XRD patterns of Sepia melanin pellets before and after the resistive switching (**Figure S8**).

### **Conflict of interest**

The authors declare no competing financial interest.

### **Corresponding Author**

\*Correspondence and requests for materials should be addressed to C.S. (email: clara.santato@polymtl.ca)



## **Author Contribution**

C. Santato and M. Reali designed the experiments. M. Reali and A. Gouda fabricated dry and wet Sepia melanin pellets. J. Bellemare designed the electrical circuit and programmed the software to measure the current-voltage characteristics of Sepia melanin pellets. M. Reali performed the current-voltage and the transient current measurements. A. Gouda acquired the electrochemical impedance spectroscopy response. C. Santato supervised the experiments. All authors gave their critical contribution to data interpretation. M. Reali and A. Gouda drafted the manuscript. All authors made comments and proofread the manuscript.

## **Acknowledgments**

Dr S. Elouatik (Raman spectroscopy), Dr J. Lefevbre (XPS), P. Plamondon (SEM and EDX) are gratefully acknowledged for technical support and discussions of the results. A. Gouda acknowledges financial support from the Institut de l'Energie Trottier and FQRNT (PBEEE) through PhD scholarships. C. Santato acknowledges financial support from NSERC (Discovery grant and Strategic Green Electronics Network: grant number: NETGP 508526-17), FQRNT (Team grant) and MESI-Quebec.

## References

- (1) Balde, C. P.; Forti, V.; Gray, V.; Kuehr, R.; Stegmann, P., *The Global E-Waste Monitor 2017. Quantities, Flows and Resources.*; United Nations University, 2017; pp 1-106.
- (2) Meloni, M.; Souchet, F.; Sturges, D., Circular Consumer Electronics: An Initial Exploration. *Ellen MacArthur Foundation* 2018; pp 1–17.
- (3) Prota, G., Melanins, Melanogenesis and Melanocytes: Looking at Their Functional Significance from the Chemist's Viewpoint. *Pigment Cell Research* **2000**, *13* (4), 283–293.
- (4) *Melanins and Melanosomes, Biosynthesis, Biogenesis, Physiological and Pathological Functions*; Patrick A. Riley, J. B., Eds.; Wiley-VCH Weinheim, Germany, 2011.
- (5) Mostert, A. B.; Rienecker, S. B.; Noble, C.; Hanson, G. R.; Meredith, P., The Photoreactive Free Radical in Eumelanin. *Science Advances* **2018**, *4* (3), 1–6.
- (6) Fedorow, H.; Tribl, F.; Halliday, G.; Gerlach, M.; Riederer, P.; Double, K. L., Neuromelanin in Human Dopamine Neurons: Comparison with Peripheral Melanins and Relevance to Parkinson's Disease. *Progress in Neurobiology* **2005**, *75* (2), 109–124.
- (7) Bettinger, C. J.; Bruggeman, J. P.; Misra, A.; Borenstein, J. T.; Langer, R., Biocompatibility of Biodegradable Semiconducting Melanin Films for Nerve Tissue Engineering. *Biomaterials* **2009**, *30* (17), 3050–3057.
- (8) Liu, Y., Ai, K., Lu, L., Polydopamine and Its Derivative Materials: Synthesis and Promising Applications in Energy, Environmental, and Biomedical Fields. *Chemical Reviews* **2014**, *114*, 5057.
- (9) Haeshin, L.; Dellatore, S. M.; Miller, W. M.; Messersmith, P. B., Mussel-Inspired Surface Chemistry for Multifunctional Coatings. *Science* **2007**, *318*, 426–430.

- (10) Lindgren, J.; Uvdal, P.; Sjövall, P.; Nilsson, D. E.; Engdahl, A.; Schultz, B. P.; Thiel, V., Molecular Preservation of the Pigment Melanin in Fossil Melanosomes. *Nature Communications* **2012**, *3*, 1–7.
- (11) Malliaras, G.; Friend, R., An Organic Electronics Primer. *Physics Today* **2005**, *58* (5), 53–58.
- (12) Di Mauro, E.; Rho, D.; Santato, C., Biodegradation of Bio-Sourced and Synthetic Organic Electronic Materials: Towards Green Organic Electronics. *Submitted*, **2020**.
- (13) Xu, R.; Gouda, A.; Caso, M. F.; Soavi, F.; Santato, C., Melanin: A Greener Route To Enhance Energy Storage under Solar Light. *ACS Omega* **2019**, *4* (7), 12244–12251.
- (14) Kim, Y. J.; Wu, W.; Chun, S. E.; Whitacre, J. F.; Bettinger, C. J., Biologically Derived Melanin Electrodes in Aqueous Sodium-Ion Energy Storage Devices. *Proceedings of the National Academy of Sciences* **2013**, *110* (52), 20912–20917.
- (15) Felix, C. C.; Hyde, J. S.; Sarna, T.; Sealy, R. C., Interactions of Melanin with Metal Ions. Electron Spin Resonance Evidence for Chelate Complexes of Metal Ions with Free Radicals. *Journal of the American Chemical Society* **1978**, *100* (12), 3922–3926.
- (16) Panzella, L.; Gentile, G.; D’Errico, G.; Della Vecchia, N. F.; Errico, M. E.; Napolitano, A.; Carfagna, C.; D’Ischia, M., Atypical Structural and  $\pi$ -Electron Features of a Melanin Polymer That Lead to Superior Free-Radical-Scavenging Properties. *Angewandte Chemie - International Edition* **2013**, *52* (48), 1–5.
- (17) Chen, C. T.; Chuang, C.; Cao, J.; Ball, V.; Ruch, D.; Buehler, M. J., Excitonic Effects from Geometric Order and Disorder Explain Broadband Optical Absorption in Eumelanin. *Nature Communications* **2014**, *5*, 1–10.
- (18) Büngeler, A.; Hämisch, B.; Huber, K.; Bremser, W.; Strube, O. I., Insight into the Final

- Step of the Supramolecular Buildup of Eumelanin. *Langmuir* **2017**, *33* (27), 6895–6901.
- (19) McGinness, J.; Corry, P.; Proctor, P., Amorphous Semiconductor Switching in Melanins. *Science* **1974**, *183* (4127), 853–855.
  - (20) Fritzsche, H., Switching and Memory in Amorphous Semiconductors, Ch. 6. In *Amorphous and Liquid Semiconductors*; Tauc, J., Ed.; Plenum Press: London and New York, 1974; pp 313–355.
  - (21) Longuet-Higgins, H. C., On the Origin of the Free Radical Property of Melanins. *Archives of Biochemistry and Biophysics* **1960**, *86*, 231–232.
  - (22) Tauc, J., Optical Properties of Amorphous Semiconductors, Ch. 4. In *Amorphous and Liquid Semiconductors*; Tauc, J., Ed.; Plenum Press: London and New York, 1974; pp 159–214.
  - (23) Powell, M. R.; Rosenberg, B., The Nature of the Charge Carriers in Solvated Biomacromolecules. *Bioenergetics* **1970**, *1* (6), 493–509.
  - (24) Di Mauro, E.; Carpentier, O.; Yáñez Sánchez, S. I.; Ignoumba Ignoumba, N.; Lalancette-Jean, M.; Lefebvre, J.; Zhang, S.; Graeff, C. F. O.; Cicoira, F.; Santato, C., Resistive Switching Controlled by the Hydration Level in Thin Films of the Biopigment Eumelanin. *Journal Material Chemistry C* **2016**, *4* (40), 9544–9553.
  - (25) Wünsche, J.; Deng, Y.; Kumar, P.; Di Mauro, E.; Josberger, E.; Sayago, J.; Pezzella, A.; Soavi, F.; Cicoira, F.; Rolandi, M.; Santato, C., Protonic and Electronic Transport in Hydrated Thin Films of the Pigment Eumelanin. *Chemistry of Materials* **2015**, *27* (2), 436–442.
  - (26) Wünsche, J.; Cicoira, F.; Graeff, C. F. O.; Santato, C., Eumelanin Thin Films: Solution-Processing, Growth, and Charge Transport Properties. *Journal Material Chemistry B*

- 2013**, *I* (31), 3836–3842.
- (27) Mostert, A. B.; Powell, B. J.; Pratt, F. L.; Hanson, G. R.; Sarna, T.; Gentle, I. R.; Meredith, P., Role of Semiconductivity and Ion Transport in the Electrical Conduction of Melanin. *Proceedings of the National Academy of Sciences* **2012**, *109* (23), 8943–8947.
  - (28) Sheliakina, M.; Mostert, A. B.; Meredith, P., Decoupling Ionic and Electronic Currents in Melanin. *Advanced Functional Materials* **2018**, 1805514.
  - (29) Sheliakina, M., Mostert, A.B., Meredith, P., An All-Solid-State Biocompatible Ion-to-Electron Transducer for Bioelectronics. *Materials Horizons* **2018**, *5* (2), 256–263.
  - (30) Salleo, A., Electronic Traps in Organic Semiconductors, Ch. 14. In *Organic Electronics: Emerging Concepts and Technologies*; Cicoira, F., Santato, C., Eds.; Wiley-VCH, 2013; pp 341–373.
  - (31) Jastrzebska, M.; Kocot, A.; Tajber, L., Photoconductivity of Synthetic Dopa-Melanin Polymer. *Journal of Photochemistry and Photobiology B: Biology* **2002**, *66*, 201–206.
  - (32) Lin, W. P., Liu, S. J., Gong, T., Zhao, Q. , Huang, W., Polymer-Based Resistive Memory Materials and Devices. *Advanced Materials* **2014**, *26*, 570–606.
  - (33) Spólnik, P.; Król, M.; Stopa, B.; Konieczny, L.; Piekarska, B.; Rybarska, J.; Zemanek, G.; Jagusiak, A.; Piwowar, P.; Szoniec, G.; Roterman, I., Influence of the Electric Field on Supramolecular Structure and Properties of Amyloid-Specific Reagent Congo Red. *European Biophysics Journal* **2011**, *40* (10), 1187–1196.
  - (34) Huggins, R. A., Simple Method to Determine Electronic and Ionic Components of the Conductivity in Mixed Conductors. A Review. *Ionics (Kiel)* **2002**, *8*, 300–313.
  - (35) Jiang, T., Hall, A., Eres, M., Hemmatian, Z., Qiao, B., Zhou, Y., Ruan, Z., Couse, A. D., Heller, W. T., Huang, H., Olvera de la Cruz, M., Rolandi, M., Xu, T., *Nature* **2020**, 577,

216.

- (36) Ferrari, A. C., Raman Spectroscopy of Graphene and Graphite: Disorder, Electron-Phonon Coupling, Doping and Nonadiabatic Effects. *Solid State Communications* **2007**, *43*, 47–57.
- (37) Saenger, K. L.; Tsang, J. C.; Bol, A. A.; Chu, J. O.; Grill, A.; Lavoie, C., In Situ X-Ray Diffraction Study of Graphitic Carbon Formed during Heating and Cooling of Amorphous-C/Ni Bilayers. *Applied Physics Letters* **2010**, *96*, 2010–2013.
- (38) Ambrico, M.; Ambrico, P. F.; Cardone, A.; Ligonzo, T.; Cicco, S. R.; Mundo, R. Di; Augelli, V.; Farinola, G. M., Melanin Layer on Silicon: An Attractive Structure for a Possible Exploitation in Bio-Polymer Based Metal-Insulator-Silicon Devices. *Advanced Materials* **2011**, *23* (29), 3332–3336.
- (39) Ambrico, M.; Cardone, A.; Ligonzo, T.; Augelli, V.; Ambrico, P. F.; Cicco, S.; Farinola, G. M.; Filannino, M.; Perna, G.; Capozzi, V., Hysteresis-Type Current-Voltage Characteristics in Au/Eumelanin/ITO/Glass Structure: Towards Melanin Based Memory Devices. *Organic Electronics* **2010**, *11*, 1809–1814.

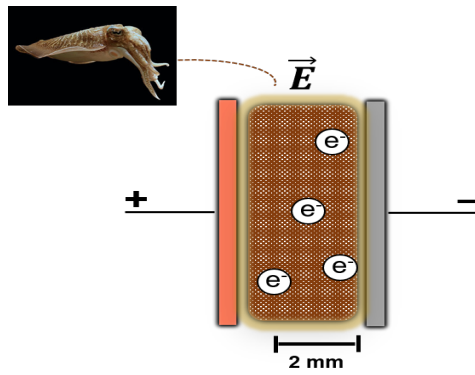
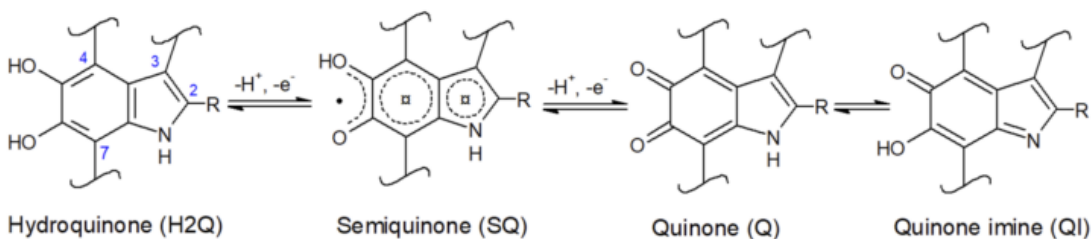
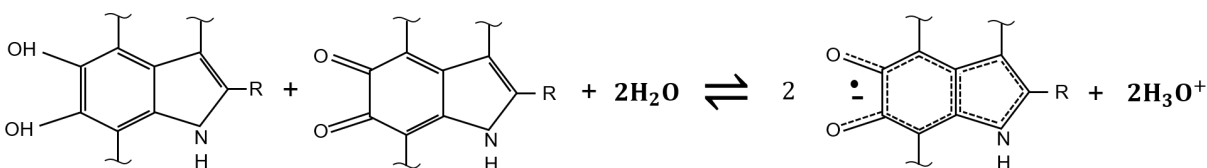


Table of content (ToC) graphic.

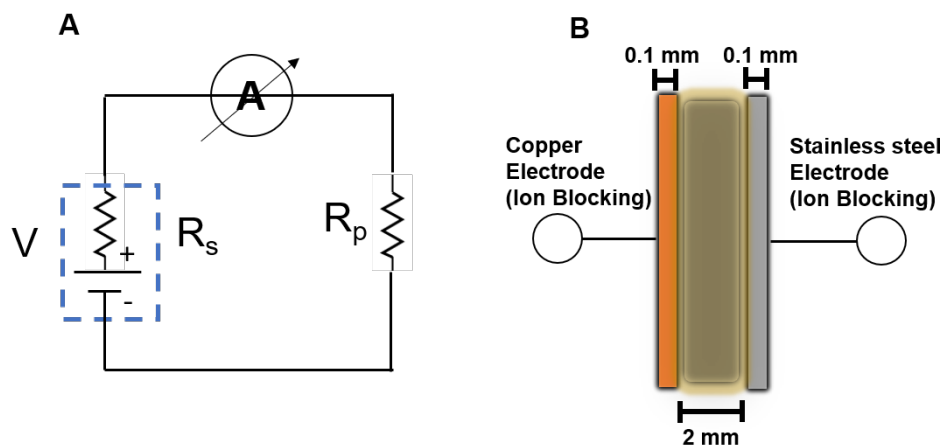


**Scheme 1.** Hydroquinone (H2Q), semiquinone (SQ) and quinone (Q) redox forms of the building blocks of eumelanin: 5,6-dihydroxyindole (DHI) and 5,6-dihydroxyindole-2-carboxylic acid (DHICA). R is –H in DHI whereas R is the –COOH group in DHICA. The quinone imine form (QI) is the tautomer of Q.

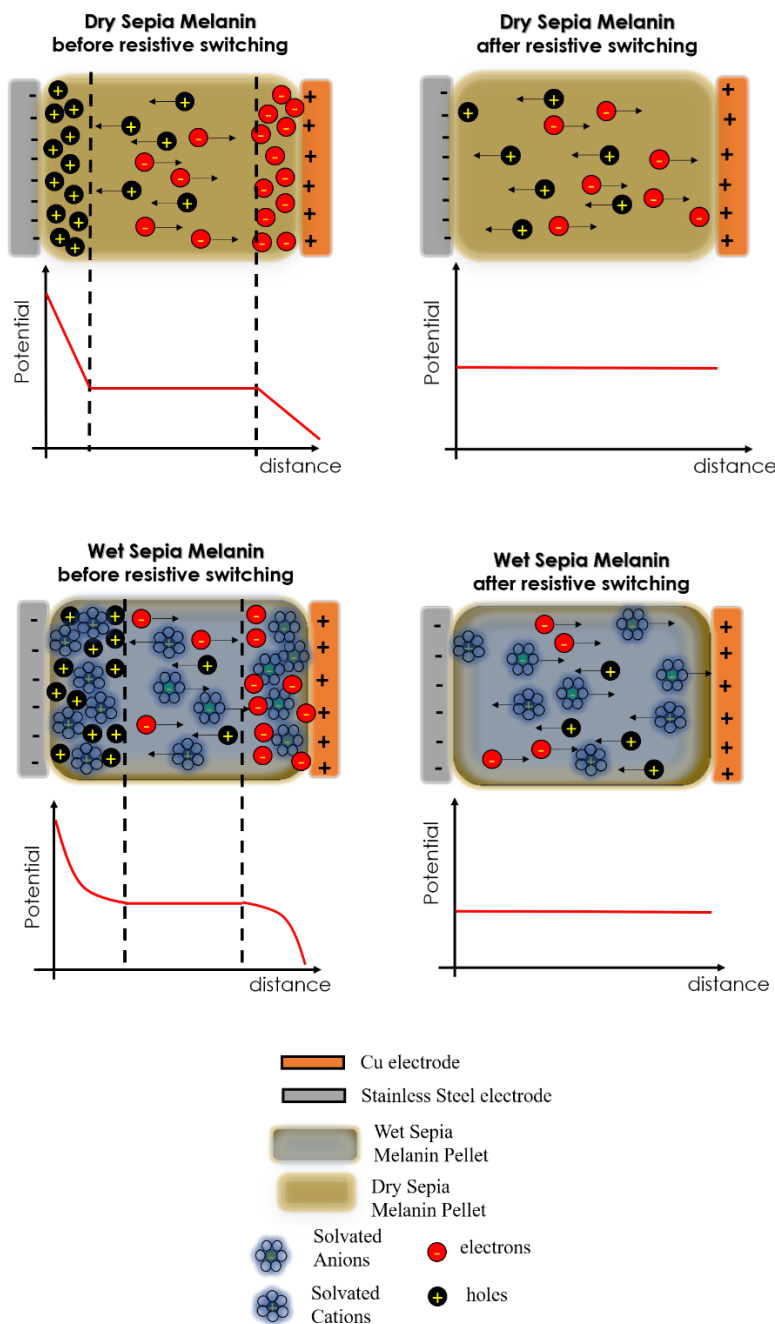


**Scheme 2.** The comproportionation equilibrium that regulates the relative concentrations of hydroquinone (H2Q), semiquinone (SQ) and quinone (Q) redox forms of the building blocks of eumelanin in the presence of water. Specifically, H2Q and Q react to form protons and SQ free radicals.





**Scheme 3.** Schematic representation of (A) the electrical circuit used in this work to acquire the electrical response of the pellets and (B) the sandwich configuration of our *Sepia melanin* pellets. In (A)  $R_s$  is the resistance of the voltage source,  $V$  is the voltage source,  $A$  is the amperometer in series with the pellet resistance  $R_p$  (including the contact resistance).



**Scheme 4.** Tentative model to describe the phenomenon of electrical resistive switching observed in dry and wet pellets of Sepia melanin, reported in this work. A key role in the model is played by the formation of electrical double layers (predominantly electronic when the pellets are dry and predominantly ionic when the pellets are wet) at the Sepia melanin /metal interfaces.

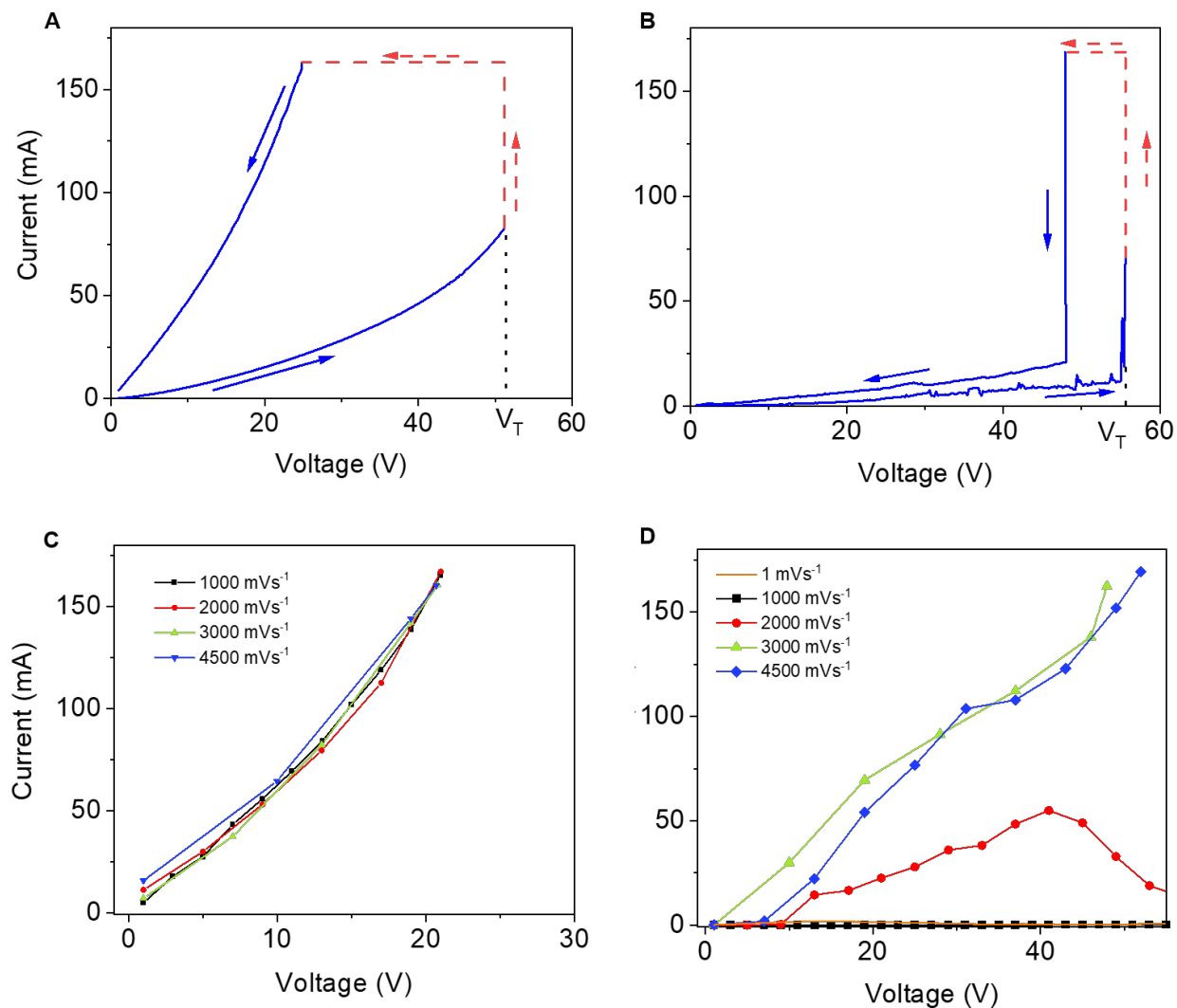


**Figure 1.** Current-voltage response at  $100 \text{ mVs}^{-1}$  for (A) dry and (B) wet pellets; sequential current-voltage acquisitions from low to high scan rates for (C) dry and (D) wet pellets (beyond  $2000 \text{ mVs}^{-1}$ , see also **Figure S2**). When the voltage source increases, the current monotonically increases up to the threshold voltage ( $V_T$ ). At  $V_T$ , because of the switching, the resistance of the pellet drops and the current increases non-monotonically up to the maximum current (maximum value of the current tolerated by the amperometer (**Scheme 3A**)). Thus, from the portion of the plot where the source voltage increases to where the source voltage decreases a transition takes place. Since this transition is fast, only its start and end points can be measured. The real

transition should appear as the contribution of a first line at constant voltage and of a second line at the constant maximum current (dash red lines and arrows).

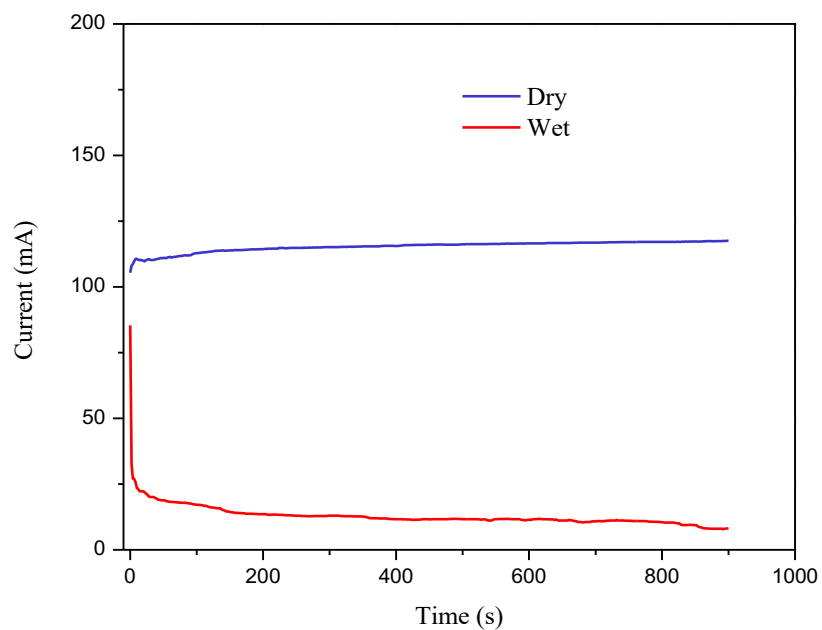


**Figure 2.** Current-time characteristics of wet and dry Sepia melanin pellets after resistive switching for dry ( $V$  is about 25 V, close to  $V_T$ ) and wet Sepia melanin pellets ( $V$  is about 45 V, close to  $V_T$ ).

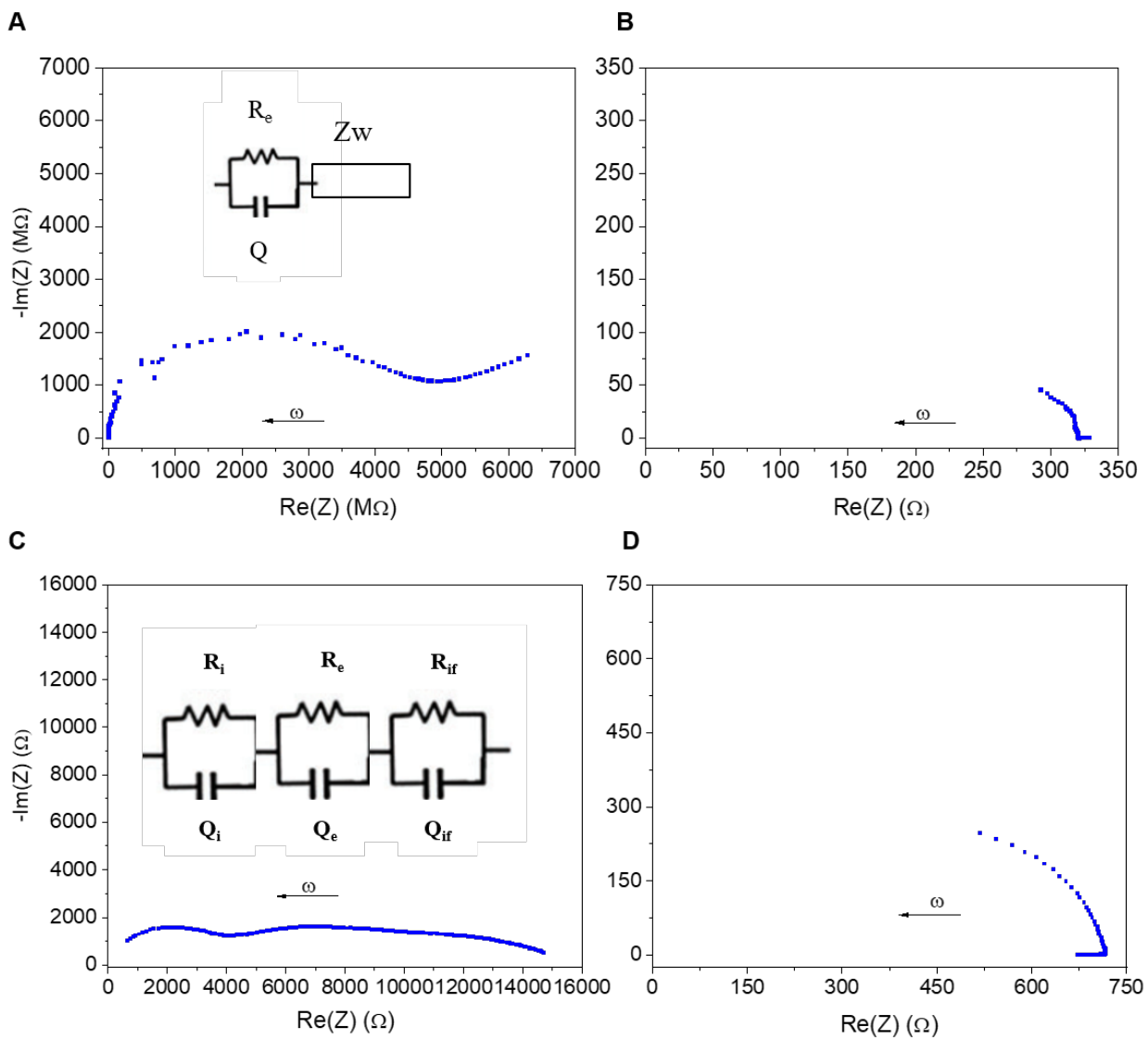


**Figure 3.** Electrochemical impedance spectroscopy of dry and wet Sepia melanin pellets. Nyquist plots of dry, (A) and (B), and wet, (C) and (D), pellets; (A) and (C) before and (B) and (D) after resistive switching. Insets of figures (A) and (C) corresponding to equivalent circuits where  $R_e$  is the electronic resistance,  $R_i$  the ionic resistance,  $R_{if}$  the interface resistance,  $Q$  is the constant phase element (the series combination of melanin's geometrical capacitance and the capacitance at melanin/metal interface that describes any deviation from an ideal capacitive response) and  $Z_w$  the diffusion hindered impedance.

Ref.	Type of eumelanin (form factor, dry versus wet)	Metal contact	Ion content	Interelectrode distance	Applied Voltage	Charge Carrier Transport Properties
19	Enzymatic action on tyrosinase, autooxidation of L-dopa, extracted from melanoma tumor material, homogenized tumor (pellets, wet)	Cu, C, Al	-	0.1, 1, 10 mm	Interval 0 V – 400 V	Electronic Conductor with Local Modification of the Dielectric Constant
27	From solutions of DL-dopa oxidized in air (pellet, 7- 16% water content)	Au	-	2 mm	15 V	Mixed Ionic-Electronic Conductor
29	From solutions of DL-dopa oxidized in air (film used as ion gating medium, wet) <sup>1</sup>	Au	-	-	-	Predominantly Ionic Conductor
38	Sigma melanin (film, 40% RH in air and vacuum)	p- or n-Si and Au	-	50 nm (diode)	ca 3 V	Predominantly Electronic Conductor
39	Sigma melanin (film, ambient conditions and vacuum)	ITO and Au	-	400 nm (diode)	ca 1.5 V	Predominantly Electronic Conductor
26	Sigma melanin (film, interval included between 50% and 90% RH)	Pt	-	10 $\mu$ m (planar configuration)	ca 1 V	Predominantly Ionic Conductor
25	Sigma melanin obtained by oxidation of tyrosine by H <sub>2</sub> O <sub>2</sub> (film, 12% and 17% water content)	Pt, Pd, PdH	-	10 $\mu$ m (planar configuration)	ca 1 V	Predominantly Ionic Conductor
24	Sigma melanin and Sepia melanin purchased from Sigma (film, 90% RH)	Au	ca 7.0 mg/g ca 64 mg/g	6 or 10 $\mu$ m (planar configuration)	ca 1 V	Ionic Conductor with Formation of Metallic Filaments
<b>This work</b>	Purified natural Sepia melanin (pellet, dry and 14% and 19% water content)	Cu and stainless steel	Cl ca 0.87 mg/g Na ca 3.9 mg/g	2 mm	Interval 0 V – 160 V	<b>Dry Pellets:</b> Electronic Conductors <b>Wet Pellets:</b> Ionic and Electronic Conductors

**Table 1.** Literature on the charge carrier transport properties of eumelanin in the form of wet and dry pellets and thin films.